
Cracks in the Foundation: A Civil Infrastructure Dataset to Challenge Vision Foundation Models

Nicola Farronato*
IBM Research
ETH Zürich
nicola.farronato@ibm.com

Niccolo Avogaro*
IBM Research
ETH Zürich
niccolo.avogaro1@ibm.com

Thomas Frick
IBM Research

Mattia Rigotti
IBM Research

Rizwan Ullah Khan
University of Twente
IBM Research

Michele Magno
ETH Zürich

Konrad Schindler
ETH Zürich

Cristiano Malossi
IBM Research

Florian Scheidegger
IBM Research

Abstract

Automated structural health monitoring is essential to prevent catastrophic infrastructure failures. Precise, pixel-level defect segmentation is needed to accurately assess structural integrity, but progress in defect segmentation for civil infrastructures has been held back by an extreme scarcity of data, which requires costly expert annotation. The need for data is accentuated by algorithmic hurdles intrinsic to the problem, including center-bias and the need to rely more on shape when inspecting nearly textureless building materials. To remove the bottleneck, we introduce **Cracks in the Foundation (CiF)**, the largest and most detailed civil infrastructure (instance) segmentation dataset to date, comprising $\approx 150,000$ high-resolution images meticulously curated over five years in collaboration with civil engineering experts. With the help of this unprecedented data source, we expose a blind spot of current visual AI: despite the advent of promptable Foundation Models (FMs) and Vision Language Models (VLMs), and despite the impressive abilities of today’s specialised segmentation models, it turns out that dense image understanding in the built environment is nowhere near solved. Our evaluations indicate that even the most recent zero-shot FMs face significant challenges when deployed on real-world infrastructure and even the performance of specialised models with domain-specific supervision plateaus at $\approx 25\%$ mAP. CiF establishes inspection of civil infrastructure, an elementary and seemingly easy perceptual task, as an open challenge that reveals fundamental weaknesses of present-day models trained predominantly on internet images, literally and figuratively highlighting *cracks in the current foundation model paradigm*.

1 Introduction

Automated structural health monitoring stands to revolutionize the maintenance of global civil infrastructure [16, 32]. In this domain, undetected defects can lead to catastrophic failures that cause massive economic damages and seriously harm humans. To assess the integrity of a structure, civil engineers require precise quantification of damage type, area, shape, and distribution. Technically,

*Equal Contribution

mapping (visible) structural damages amounts to a pixel-level segmentation problem. Given the high stakes and the complex physics of materials and their failure, high accuracy is required before a system can be deployed in the real world.

Training as well as evaluation of segmentation methods for civil infrastructure have been hobbled by data scarcity, and complicated by algorithmic peculiarities compared to general-purpose image segmentation [2]. Datasets at the scale needed for contemporary machine learning are lacking, as crowdsourcing is not practical when annotators must have the expertise to distinguish microscopic deterioration from harmless shadows. Yet, it is not just a data problem: we will show that even with abundant data, the domain exposes fundamental weaknesses in modern visual AI architectures: the monochromatic, flat appearance of concrete means that understanding must rely on shape rather than texture, a notorious weakness of deep learning models [18]. The issue is further exacerbated by thin, highly non-convex target structures incompatible with the models’ known center-bias [48].

To plug this critical gap, we introduce Cracks in the Foundation (CiF), illustrated in Figure 1, a civil infrastructure dataset with instance annotations that is the largest of its kind in terms of both volume and resolution, consisting of $\approx 150,000$ images and $\approx 250,000$ fine-grained masks. Curated and meticulously annotated over five years of direct collaboration between AI industry partners and civil engineering experts, CiF captures the full scale range and visual complexity of infrastructure “in the wild.” By open-sourcing this unprecedented collection, we provide a rigorous, analysis-ready benchmark that exposes the limits of modern vision models. We hope to challenge the community and to ultimately foster the development of visual AI capable of safeguarding our physical environment.

Cracks in the Foundation especially point at an issue that has been largely overlooked in the recent AI boom. The advent of Vision Language Models [1, 30, 5, 27, 33] (VLMs), especially those capable of visual grounding [37, 14, 46, 38, 25, 6, 12], and of promptable Foundation Models [23, 39, 10, 31] (FMs) has to some degree created the illusion that dense image understanding is solved [4]. Applying these models to the civil infrastructure domain reveals a serious, unexpectedly strong limitation: zero-shot generalization falls remarkably short. Cutting-edge FMs, trained predominantly on internet-scraped image collections like COCO [29] or LAION [43], seem to lack understanding of the features and scale variations needed in civil engineering applications. Experiments with our benchmark demonstrate that state-of-the-art promptable models fail to identify structural anomalies, and even domain-specific, supervised models plateau at $\approx 25\%$ mAP. In other words, segmenting civil infrastructure degradations is, despite its straightforward nature, an open problem for present-day visual AI and challenges current solutions, literally revealing *cracks in the foundation* model paradigm.

2 Related Works

Large-scale benchmarks have catalyzed modern computer vision [41, 43], with dense prediction datasets like MSCOCO [29], ADE20K [49], and SA-1B [23] demonstrating that high-quality instance masks are essential for training robust object detection and segmentation architectures. However, civil infrastructure inspection remains a highly specialized outlier. In this domain, generic features consistently fail to capture critical, fine-grained anomalies—such as subtle crack patterns or complex concrete deterioration—under variable real-world conditions.

To address these domain-specific needs, the civil infrastructure landscape has seen a proliferation of datasets, as comprehensively surveyed by Bianchi and Hebden [9], who cataloged 86 datasets up to 2022. These resources have evolved through levels of increasing annotation complexity, although the vast majority remain restricted to classification or semantic segmentation tasks. Early efforts primarily provided image-level or patch-level labels; for example, CDS [19] and SDNET2018 [15] focused on binary crack detection in concrete patches. More comprehensive multi-class datasets like MCDS [20] and multi-label benchmarks like CODEBRIM [34] expanded these to multiple reinforced concrete defect types. Pixel-level semantic segmentation has further matured this landscape, with single-class crack datasets like UAV75 [7] and CrackSeg9k [24] providing large-scale binary masks. Recent state-of-the-art resources such as S2DS [8] and dacl10k [17] represent the current pinnacle of this progression, with dacl10k offering 9,920 images across 19 classes for semantic bridge damage segmentation.

Despite this growth, instance segmentation remains significantly underdeveloped in the civil infrastructure landscape. While semantic segmentation identifies defect types, it does not distinguish

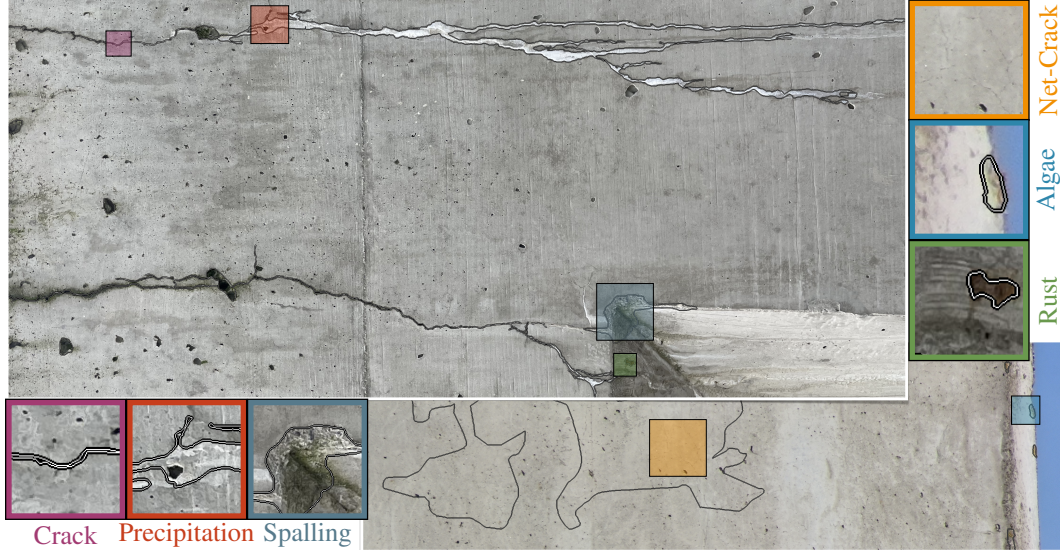


Figure 1: Representative high-definition images from Cracks in the Foundation dataset. Due to the high resolution of the imagery and the fine scale of the structural anomalies, magnified callouts are utilized to visualize specific defect classes: Crack (magenta), Precipitation (red), Spalling (blue), Net-Crack (orange), Algae (cyan), and Rust (green).

between separate occurrences, which is critical for damage quantification and structural health tracking. The few existing instance-level datasets suffer from substantial limitations in terms of scale, resolution, and class diversity. For instance, MCrack1300 [45] provides instance masks for only 1,300 masonry images, while CConCrack [3] offers a limited core set of 400 images for cracks and spalls. Most existing instance datasets focus on a single defect class (predominantly cracks) and lack the large-scale volume of images necessary to train contemporary instance segmentation models effectively.

Table 1 provides a comparative summary of the most influential datasets in this field alongside our proposed work, reporting both native full-scene parameters and derived patch-level metrics. Among classification benchmarks, SDNET2018 [15] and CODEBRIM [34] offer high native resolutions (up to 24 MPx) but rely on low-resolution patches (≤ 0.06 MPx) for primary tasks. In semantic segmentation, CrackSeg9k [24] aggregates over 2,000 images from ten sources into a 0.16 MPx patch benchmark, while dacl10k [17] remains the largest full-scene resource with 9,920 images at 3.10 MPx. Current instance-level efforts like CConCrack [3] (augmented from 400 core images) represent early steps toward defect isolation but are often limited in scale or class diversity. Our CiF dataset addresses these gaps by providing 12,896 high-resolution (16.66 MPx) images with 148,642 high-fidelity patches (1.05 MPx), representing the first large-scale, multi-class instance segmentation benchmark for bridge inspection that preserves fine-grained detail across both release variants.

3 Dataset Details

3.1 Data acquisition

Collected over five years in collaboration with infrastructure owners (Sund & Bælt, Trafikverket, Zurich Kanton), the dataset focuses on European civil infrastructure, particularly bridges. Its hybrid design combines heterogeneous “in-the-wild” field data to capture real-world variability with controlled inspection setups for structured, repeatable imaging. This dual approach ensures broad structural and environmental diversity, ultimately supporting robust model training and reliable evaluation.

In-the-Wild Data. The in-the-wild subset (26% of the data) was collected collaboratively by engineers and researchers during routine inspections of operational infrastructure. Images were

Table 1: Comparison of our dataset parameters with other civil infrastructure defect datasets. For image counts and resolution, we report both the original full-scene data and the derived patches/augmented samples where applicable.

Dataset	Task	Classes	Images		Resolution (MPx)	
			Full	Patches	Full	Patch
SDNET [15]	Classification	1	230	56,092	14.06	0.06
CODEBRIM [34]	Classification	5	1,590	7,733	24.00	0.05
GYU-DET [28]	Classification	6	11,123	–	15.93	–
CrackSeg9k [24]	Semantic seg.	1	2,003	9,255	0.25	0.16
S2DS [8]	Semantic seg.	6	743	–	1.05	–
dacl10k [17]	Semantic seg.	19	9,920	–	3.10	–
Özgenel [36]	Instance seg.	1	458	–	12.19	–
MCrack1300 [45]	Instance seg.	5	1,300	–	0.41	–
CConCrack [3]	Instance seg.	2	400	10,995	12.19	1.05
CiF (Ours)	Instance seg.	6	12,896	148,642	16.66	1.05

acquired in unconstrained field conditions using a variety of consumer-grade and industrial camera systems. Consequently, this subset exhibits substantial variability in resolution, viewpoint, illumination, weather conditions, and scene composition. This variability reflects the diversity of real-world inspection scenarios and is intentionally retained to improve model generalisation. In particular, the dataset includes a wide range of defect manifestations across different structural contexts, enabling evaluation under realistic deployment conditions.

Controlled Inspection Setups. Complementing our in-the-wild data, we utilized drone-assisted controlled acquisitions to safely gather scalable, repeatable imagery in difficult environments. To simultaneously maximize structural surface coverage and ensure sufficient pixel density for fine-grained defect detection, we employed two distinct flight modes: a scan setup and a high-resolution setup. Detailed drone and camera specifications are provided in Table 2.

Table 2: Overview of camera systems and lens configurations used in the controlled inspections.

Camera	System type	Focal length [mm]	Zoom / lens	Resolution
DJI ZH20/ZH20T	Optical zoom	6.83–119.94 (opt.)	23× opt., 200× digital	5184 × 3888
DJI Zenmuse X7	Prime lens (S35)	50 (used; 16/24/35/50 avail.)	Fixed lens	6016 × 3376
DJI Zenmuse P1	Prime lens (FF)	50 (used; 24/35/50 avail.)	Fixed lens	8192 × 5460

Scan Setup. Prioritizing efficient, large-scale coverage over maximal detail, the scan setup utilizes a drone flying parallel to the target surface with a perpendicular camera. Operating in downward, vertical, or upward-facing orientations, the drone typically executes a zigzag trajectory to ensure systematic coverage, simultaneously recording high-precision GPS/RTK data to enable the accurate spatial registration of the captured imagery.

High-Resolution Setup. In the high-resolution setup, the drone remains in a stationary hover position while using a gimbal-mounted camera to capture a structured grid of zoomed-in images of the target surface. This approach prioritises fine-grained visual detail. To enable reconstruction of larger surface regions, we assume no oblique views so that homography transformations are used to map local views into a shared reference frame, enabling mosaic reconstruction of the observed area. This setup is particularly suitable for detailed inspection of localized structural regions where high spatial resolution is required for defect inspection. A representative hardware configuration includes the DJI Matrice 300 RTK² equipped with a Zenmuse H20T³, although the proposed acquisition

²<https://enterprise.dji.com/matrice-300>

³<https://enterprise.dji.com/zenmuse-h20-series/specs>

methodology is not restricted to specific hardware and can be implemented with comparable sensor systems.

3.2 Images, Classes and Dataset Splits

The dataset contains 12,896 native high-resolution images (0.23 to 42.18 MPx, mean 16.66 MPx) annotated for six defect categories defined jointly with civil engineers. Unlike most defect benchmarks that release pre-cropped or downsampled patches, we preserve the native resolution: hairline cracks down to a few pixels in width are polygonally annotated within multi-megapixel inspection images, alongside spatially extensive defects such as algae colonisations covering large portions of a single frame. We release two coordinated variants: *Full* preserves the native resolution and *Tiled* partitions every image into 1024×1024 patches (148,642 in total) using the procedure described in §3.3, providing a uniform-resolution benchmark suitable for current vision backbones.

Classes. The six categories covering the dominant visual defect families on aged concrete and steel surfaces are illustrated in Figure 2. *Algae*: biological surface growth indicating sustained moisture. *Crack*: linear discontinuities in the concrete or coating. *Net-Crack*: interconnected polygonal cracking patterns (alligator or map cracking) associated with fatigue or shrinkage. *Crack with Precipitation*: crack with mineral deposits left by water seepage (efflorescence). *Rust*: oxidation of exposed or embedded steel reinforcement. *Spalling*: detachment or fragmentation of surface material.



Figure 2: Mosaic of the six defect types in tiled images.

Splits. Images are partitioned into train (70%), validation (15%), and test (15%) at the source-image level, and tiles inherit the split of their parent image, so no content leaks between splits across resolutions. The Full variant contains 12,896 images (9,096 train, 1,942 val, 1,858 test), while the Tiled variant provides 148,642 patches (105,139 train, 22,368 val, 21,135 test). We have fully open-sourced the dataset, providing public access to the native images, tiled partitions, and official evaluation splits.

3.3 Annotation Procedure

All defects are annotated as instance-level polygon masks at native image resolution, capturing both hairline cracks a few pixels wide and large-extent defects spanning a substantial fraction of multi-megapixel frames. The class taxonomy of §3 was finalised in close collaboration with civil engineers at Sund & Bælt, restricted to six categories that are simultaneously severe enough to warrant pixel-level localisation and operationally actionable for structural inspection and maintenance. Polygon mask annotation was carried out by an external annotation vendor under written guidelines authored jointly with the domain experts, with quality assurance performed both internally by the vendor and by our in-house reviewers.

Annotation guidelines. A written guideline document was produced for the annotation team, defining each defect type by a textual description, positive examples, and characteristic false positives. Because defect appearance, scale, and confusable background structures vary markedly across acquisition modalities and asset classes, separate guideline variants were issued per image source (drone, phone camera, DSLR) and per structure type (concrete bridge, city infrastructure, etc.). The guidelines were maintained as a living document throughout the five-year campaign: ambiguous samples surfaced by the annotation team were triaged with the domain experts and, once resolved, folded back as new canonical examples. This loop is the primary mechanism by which we controlled the dominant source of label noise in this domain—defect ambiguity at the boundary between visually similar categories.

Pre-annotation triage. Two classes of images were excluded prior to annotation. Frames judged to be of insufficient image quality (motion blur, severe defocus, or extreme exposure) were discarded. Frames that contained no defect of interest were treated as background and excluded from the annotated set; they do not contribute to the released splits.

Batches and pilot phase. Annotation proceeded in batches of approximately 500–1,000 images, grouped by image source and structure type, which we refer to as a *batch type*. For every new batch type, the annotation team first delivered a pilot of 10–50 images, used both to calibrate annotators to the specific imaging conditions and structure and to surface guideline gaps before they propagated through a full batch. Pilots were reviewed end-to-end and iterated upon with the team until quality was acceptable; a full batch was released only after pilot sign-off.

Full-batch annotation and QA. Full batches were produced by an external annotation vendor, who performed an internal first-pass QA before delivery. On delivery, our in-house ML research team—trained by the domain experts mainly at Sund & Bælt—performed a second-pass review by spot-checking approximately 10% of images at the instance level. A batch was rejected and returned for a further correction pass if the spot-check yielded an instance-level false-positive or false-negative rate above the contractually defined threshold of 10%; otherwise, the specific errors identified during the spot-check were corrected, and the batch was accepted. As a bootstrap, the first five batches were reviewed in full rather than via spot-check, which served both to calibrate the in-house reviewer pool against the guideline and to verify that the 10% spot-check was representative of overall batch quality before being relied on subsequent batches.

3.4 Statistics

The *Full* variant is characterized by its high native resolution, which significantly exceeds that of standard generic instance segmentation benchmarks. With a mean of 16.66 MPx and a median of 20.16 MPx, the images are approximately 50× larger than COCO (~0.3 MPx) [29] and 8× larger than Cityscapes (2.1 MPx) [13]. The cumulative distribution shown in Fig. 4b reveals that approximately 70% of the images have a resolution of at least 20 MPx, reflecting the raw output of operational field hardware: smartphones, DSLRs, and gimbal-mounted survey cameras. Such high resolution is essential to capture hairline defects and high-frequency structural textures that would be lost in standard downsampled benchmarks.

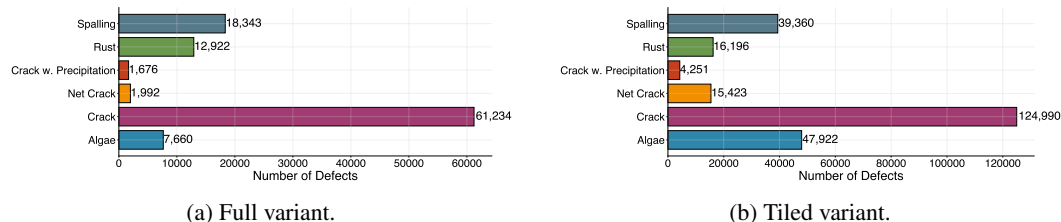


Figure 3: Per-class defect instance counts in the Full and Tiled variants.

Instance Density and Class Distribution. The dataset contains a total of 103,827 defect instances in the Full variant. On average, each image contains 8.05 instances, a density that is higher than

both generic benchmarks like COCO [29] (~ 7.3 instances/image) and specialized infrastructure benchmarks like CODEBRIM [34] (~ 3.37 instances/image). The class distribution is strongly long-tailed (Fig. 3). In the Full variant, Crack accounts for 59.0% of all instances, while Spalling and Rust represent 17.7% and 12.5% respectively. Rarer categories such as Net-Crack (1.9%) and Crack with Precipitation (1.6%) still provide nearly two thousand instances each (Net-Crack: 1,992, Precipitation: 1,676 in Full). The Tiled variant exhibits a different distribution due to the partitioning of spatially extensive defects: Algae rises to 19.3% of instances, while Crack and Spalling account for 50.4% and 15.9% respectively.

Defect Scale and Geometric Diversity. Beyond image scale, the difficulty profile is dominated by the wide span of defect instance areas across and within classes. Median instance areas span over two orders of magnitude across categories: from ~ 2.3 K px^2 for Rust to ~ 807 K px^2 for Net-Crack. Intra-class spread is exceptionally large, with Crack instances ranging over six orders of magnitude in area (Fig. 4a). While the Full variant preserves these extremes, the Tiled variant filters out small defects (minimum area ~ 0.5 K px^2) and partitions large defects (e.g., Algae and Net-Crack) into many tiles. Furthermore, the defects exhibit high geometric diversity. While Cracks are characteristically elongated (mean aspect ratio 4.4), Algae and Net-Cracks often cover irregular, spatially extensive areas with higher compactness (0.67 and 0.85, respectively, in Full). This structural variety prevents models from relying on simple shape priors and requires robust spatial reasoning across multiple scales.

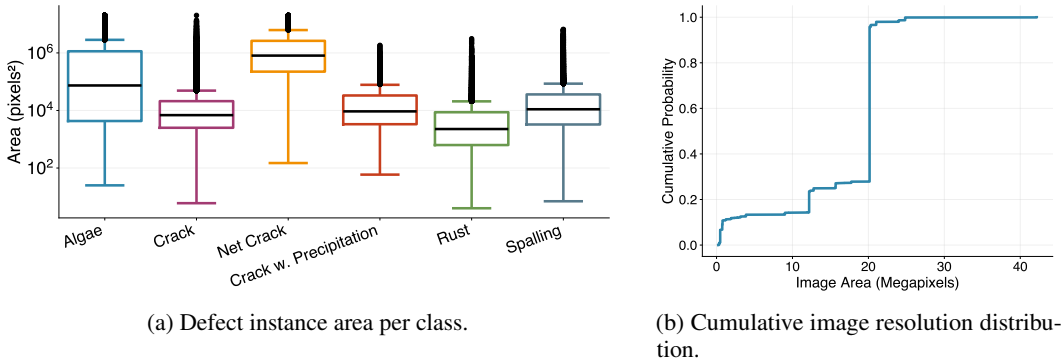


Figure 4: Quantitative properties of the Full variant: distribution of defect areas across classes (a) and cumulative native image resolution distribution (b).

Baselines in this paper operate on the Tiled variant; the Full variant is released to support evaluation of resolution-aware and tile-aggregation methods. Class co-occurrence and per-class shape compactness are reported in Appendix A.

4 Evaluation

Supervised baselines. To establish rigorous baselines on the CiF dataset, we evaluate a diverse suite of state-of-the-art architectures renowned for top-tier performance on standard instance segmentation benchmarks like COCO. Our selection strategically covers three distinct paradigms: (i) Industry Standards: We include the YOLO family (specifically YOLOv11 [22] and YOLOv26 [42]) as the de facto standards for real-world, high-performance segmentation; (ii) DETR-Based Architectures: We evaluate Mask DINO [26] as a strong DETR-based [11] segmentation and detection baseline, alongside RF-DETR [40], a state-of-the-art compact and computationally efficient transformer model; and (iii) Pretrained Foundations: We include EoMT [21] to assess knowledge transfer of strong, pretrained foundational encoders to the civil infrastructure domain. Specifically, we aim to probe the out-of-domain finetuning of foundation backbones like DINOv2/v3 [35, 44] using a state-of-the-art algorithm like EoMT. All baselines are fully fine-tuned on the CiF training split, starting from standard pretrained weights if available with optimal checkpoints selected via validation performance before final evaluation on the held-out test set. The results are detailed in Table 3, reporting the $\text{mAP}_{50:95}$ performance for both the instance segmentation masks and the bounding box predictions. More details about the training setups can be found in Appendix A.1.

Table 3: Object detection (bb) and instance segmentation (seg) results for supervised baselines on the CiF dataset. Models were trained on the training set, and the best-performing checkpoint on the validation set was used for final evaluation on the test set.

Method	Encoder	$mAP_{50:95}$		$AP_{50:95}$											
				Algae		Crack		Net-Crack		Precipitation		Rust		Spalling	
		bb	seg	bb	seg	bb	seg	bb	seg	bb	seg	bb	seg	bb	seg
Mask-DINO [26]	Resnet-50	29.0	20.4	51.2	46.5	31.3	3.0	27.2	22.8	14.1	4.3	26.9	26.7	23.4	19.0
YOLOv11 [22]	nano	31.0	19.8	52.6	43.6	31.0	6.5	29.0	21.0	17.1	4.9	30.0	25.1	26.1	17.7
	small	32.3	20.7	53.0	43.9	32.9	7.5	29.2	21.7	18.3	5.9	32.8	26.7	27.4	18.7
	medium	33.2	21.5	53.4	44.3	34.6	8.2	30.2	23.2	18.8	6.3	34.0	27.4	28.4	19.7
	large	33.9	21.9	53.8	44.7	35.6	8.5	30.8	23.5	19.9	6.7	34.7	27.8	29.2	20.3
	xlarge	33.9	21.9	53.6	44.3	35.6	8.6	30.7	23.4	19.7	7.2	35.0	28.2	28.7	19.9
YOLOv26 [42]	nano	30.2	19.5	52.0	43.5	30.3	6.8	27.8	20.7	17.4	4.9	28.2	23.6	25.2	17.4
	small	32.2	20.9	52.7	43.9	32.5	7.6	29.1	21.8	19.6	7.0	31.7	25.9	27.6	19.0
	medium	32.8	21.4	53.0	44.3	33.2	8.1	29.8	22.9	20.2	6.9	33.3	27.3	27.3	19.1
	large	32.0	20.2	51.7	42.8	33.1	7.9	27.5	20.4	20.1	6.3	32.4	25.6	26.8	18.5
	xlarge	32.7	21.0	52.2	43.4	34.1	8.9	27.2	20.6	20.1	6.8	33.7	26.2	28.9	20.3
RF-DETR [40]	nano	35.3	18.3	59.3	46.1	37.5	1.2	30.6	21.5	18.6	7.3	36.4	16.7	29.7	17.1
	small	36.2	18.2	59.2	46.2	38.3	1.3	31.8	21.4	20.5	7.2	36.8	17.4	30.5	15.8
	medium	35.7	18.3	59.1	46.8	38.1	1.2	31.5	21.5	19.6	6.8	36.4	17.0	29.7	16.7
	large	35.7	18.3	58.9	46.5	38.2	1.3	31.5	21.0	19.5	7.6	36.5	16.7	29.8	16.6
EoMT [21]	DinoV3	32.9	24.2	57.0	49.6	28.4	4.7	30.4	24.1	17.9	10.3	34.8	31.6	29.2	25.1
	DinoV2	32.7	24.1	56.4	48.8	29.0	5.0	29.3	23.5	16.8	9.5	35.2	32.6	29.6	25.2

Foundation Model Evaluation. Given the recent success of Foundation Models (FMs) and Vision-Language Models (VLMs) claiming universal, zero-shot detection and segmentation capabilities [23, 25, 6], we conduct a rigorous evaluation of these architectures on the CiF dataset. We specifically investigate two dominant paradigms: promptable segmentation and zero-shot object detection. For promptable segmentation, we evaluate SAM3 [10], the latest iteration of the Segment Anything family [23, 39]. To thoroughly assess its adaptability, we evaluate SAM3 under three distinct prompting protocols: oracle bounding boxes derived from ground truth, oracle point-based prompting (randomly sampling 1 to 5 points from the ground truth mask), and text-based prompting. For zero-shot detection, we evaluate Qwen3-VL, a state-of-the-art VLM known for exceptional performance on referring expression segmentation benchmarks (e.g., refCOCO, refCOCO+ [47]) and diverse vision-language tasks. Qwen3-VL is evaluated using standard off-the-shelf text prompts, instructed to output object detections in a structured JSON format. Moreover, we benchmark SAM3-Agent, a hybrid architecture integrating the zero-shot reasoning capabilities of Qwen3-VL with the precise dense prediction of SAM3 within an agentic framework. Quantitative results are detailed in Table 4 for instance segmentation and bounding box detection, with both evaluated using the $mAP_{50:95}$ metric.

4.1 Discussion

Moderate success of supervised baselines. Standard supervised models achieve reasonable object detection performance, yielding an overall bounding-box $mAP@50:95$ of approximately 35%. The models exhibit strong localization capabilities on visually distinct, surface-level anomalies such as algae (reaching up to 59% mAP). However, performance degrades on critical structural defects. Complex failure modes, such as *net crack* or *crack with precipitation*, yield localization scores of only 20–30%, showing all the challenges of the civil infrastructure domain. When it comes to instance segmentation, performance drops drastically across all architectures. With the exception of high-contrast algae, mask mAP plunges to single digits for fine-grained structural defects like cracks. This drop in pixel-level accuracy is particularly detrimental for civil engineering applications, where the severity of a defect is strictly measured by its exact geometric footprint. Among the segmentation baselines, EoMT achieves the highest performance by leveraging an internet-scale foundational backbone. This outcome suggests that massive-scale pretraining may offer a measurable advantage in feature extraction, though it is difficult to cleanly disentangle the impact of the foundational data from the model’s inherent architecture. What remains definitively clear, however, is that the absolute performance is insufficient for real-world application. This stark reality positions CiF as a vital asset and proving ground, challenging the field to determine whether future breakthroughs in civil

Table 4: Performance comparison of SAM3 and Qwen3-VL on the CiF dataset. The $AP_{50:95}$ metric denotes segmentation accuracy for SAM3 and object detection accuracy for Qwen3-VL.

Method	$mAP_{50:95}$	$AP_{50:95}$					
		Algae	Crack	Net-Crack	Precipitation	Rust	Spalling
SAM3-Agent	1.7	1.0	0.7	0.0	1.0	7.0	0.7
SAM3-Text	2.0	1.0	0.7	0.0	1.6	8.8	0.0
SAM3-Oracle #1 point	7.8	10.4	0.4	6.7	3.0	18.1	8.2
SAM3-Oracle #3 points	16.1	30.5	0.6	20.9	4.6	25.5	14.7
SAM3-Oracle #5 points	18.6	33.9	0.8	25.0	5.8	28.2	17.9
SAM3-Oracle Bounding Box	34.2	56.0	1.9	54.1	10.4	46.0	37.1
Qwen3-VL-4B	1.5	4.7	2.4	0.1	0.1	1.4	0.5
Qwen3-VL-8B	1.9	5.8	2.0	0.1	0.1	2.8	0.4
Qwen3-VL-32B	2.0	6.7	2.8	0.4	0.1	1.3	0.6
Qwen3-VL-235B-A22B	2.4	7.3	3.3	0.7	0.1	2.3	0.8

infrastructure will be driven by specialized architectural advancements or by even larger, high-fidelity datasets.

The Illusion of Zero-Shot Generalization. Our evaluation of Foundation Models and VLMs reveals poor zero-shot performance, exposing a critical gap between benchmark success and real-world utility. For instance, despite its massive scale, the Qwen3-VL (235B-A22B) model fundamentally fails at zero-shot object detection on civil infrastructure, yielding an abysmal mean bounding box mAP of just 2.4%. SAM3 fares no better in zero-shot dense prediction. Even when evaluated under oracle conditions (using ground-truth bounding boxes or point prompts), performance remains strikingly low except for large defects. The model struggles with the fine-grained predictions required for the “crack” class, confirming that generic segmentation foundations lack the specific priors necessary for defect segmentation. Consequently, these limitations undermine SAM3’s viability as an automated annotation assistant, further reinforcing the extreme difficulty and expense of curating high-fidelity training data in this domain.

Cracks in the Foundation. The evaluation experiments point to an overlooked, yet vital issue in current ML literature: models that achieve state-of-the-art results on curated, general-purpose datasets consistently fail to generalize to complex, real-world domains such as civil infrastructure visual inspection. The primary objective of CiF is to spotlight this deficiency and open-source a massive-scale dataset to close this gap. Given the profound societal and economic impact of automated structural health monitoring, resolving this domain shift is not just a theoretical machine learning challenge, but a critical real-world necessity.

4.2 Limitations

While CiF represents a large-scale and relevant dataset for civil infrastructure defect segmentation, several limitations remain. First, the dataset focuses primarily on bridge structures and concrete materials in Europe, and therefore does not fully represent the diversity of global infrastructure systems, such as steel or underground structures. Second, defect annotation is inherently subjective, particularly for fine-grained or low-contrast damage patterns, which may introduce variability even among expert annotators. Third, the data acquisition process—combining in-the-wild imagery with controlled drone-based inspections—may introduce biases in viewpoint, scale, and sensor characteristics. In addition, the dataset reflects a long-tailed distribution of defect types, which may impact model performance across rare categories. Lastly, despite its unprecedented scale, CiF remains vastly smaller than general-purpose datasets like LAION [43]. While our evaluation exposes severe model failures, the root cause remains an open question. We cannot prove whether these limitations are strictly architectural; it is possible that scaling the dataset by several orders of magnitude could resolve them, though such an effort is currently economically prohibitive.

5 Conclusions

We introduce Cracks in the Foundation (CiF), the largest high-resolution instance segmentation dataset for civil infrastructure to date. Evaluations on CiF suggest the domain remains highly challenging: state-of-the-art Foundation Models struggle with zero-shot generalization, and specialized models plateau below real-world requirements. Ultimately, CiF establishes structural health monitoring as an open, unsolved challenge. By open-sourcing this unprecedented benchmark and large-scale training dataset, we empower the community to develop robust architectures capable of genuinely safeguarding our physical world.

Acknowledgments and Disclosure of Funding

We would like to sincerely thank Finn Bormlund and Svend Gjerding (Sund & Baelte), Jens Hägström (Trafikverket), Raphael von Thiessen (Innovation-Sandbox for AI, Office for Economy, Kanton Zürich), and the Dübendorf Air Base for granting us the opportunity to collect, analyze, and disseminate the images and defect data included in this publication. We acknowledge funding from the European Union’s Horizon Europe research and innovation programme under the Marie Skłodowska-Curie actions HORIZON-MSCA-2022-DN-01 call (Grant agreement ID: 101119554) to Nicola Farronato and Rizwan Ullah Khan, and Horizon Europe grant No. 101070408 (SustainML) to Niccolo Avogaro and Mattia Rigotti.

References

- [1] Jean-Baptiste Alayrac, Jeff Donahue, Pauline Luc, Antoine Miech, Iain Barr, Yana Hasson, Karel Lenc, Arthur Mensch, Katie Millican, Malcolm Reynolds, Roman Ring, Eliza Rutherford, Serkan Cabi, Tengda Han, Zhitao Gong, Sina Samangooei, Marianne Monteiro, Jacob Menick, Sebastian Borgeaud, Andrew Brock, Aida Nematzadeh, Sahand Sharifzadeh, Mikolaj Binkowski, Ricardo Barreira, Oriol Vinyals, Andrew Zisserman, and Karen Simonyan. Flamingo: a visual language model for few-shot learning, 2022.
- [2] Palisa Arafin, Ahm Muntasir Billah, and Anas Issa. Deep learning-based concrete defects classification and detection using semantic segmentation. *Structural Health Monitoring*, 23(1):383–409, Jan 2024.
- [3] Saeid Ataei, Saeed Adibnazari, and Seyyed Taghi Ataei. Data-driven detection and evaluation of damages in concrete structures: Using deep learning and computer vision. *arXiv preprint arXiv:2501.11836*, 2025.
- [4] Niccolo Avogaro, Thomas Frick, Mattia Rigotti, Andrea Bartezzaghi, Filip Janicki, Cristiano Malossi, Konrad Schindler, and Roy Assaf. Show or tell? effectively prompting vision-language models for semantic segmentation, 2025.
- [5] Jinze Bai, Shuai Bai, Shusheng Yang, Shijie Wang, Sinan Tan, Peng Wang, Junyang Lin, Chang Zhou, and Jingren Zhou. Qwen-vl: A versatile vision-language model for understanding, localization, text reading, and beyond, 2023.
- [6] Shuai Bai, Yuxuan Cai, Ruizhe Chen, Keqin Chen, Xionghui Chen, Zesen Cheng, Lianghao Deng, Wei Ding, Chang Gao, Chunjiang Ge, Wenbin Ge, Zhifang Guo, Qidong Huang, Jie Huang, Fei Huang, Binyuan Hui, Shutong Jiang, Zhaohai Li, Mingsheng Li, Mei Li, Kaixin Li, Zicheng Lin, Junyang Lin, Xuejing Liu, Jiawei Liu, Chenglong Liu, Yang Liu, Dayiheng Liu, Shixuan Liu, Dunjie Lu, Ruilin Luo, Chenxu Lv, Rui Men, Lingchen Meng, Xuancheng Ren, Xingzhang Ren, Sibao Song, Yuchong Sun, Jun Tang, Jianhong Tu, Jianqiang Wan, Peng Wang, Pengfei Wang, Qiuyue Wang, Yuxuan Wang, Tianbao Xie, Yiheng Xu, Haiyang Xu, Jin Xu, Zhibo Yang, Mingkun Yang, Jianxin Yang, An Yang, Bowen Yu, Fei Zhang, Hang Zhang, Xi Zhang, Bo Zheng, Humen Zhong, Jingren Zhou, Fan Zhou, Jing Zhou, Yuanzhi Zhu, and Ke Zhu. Qwen3-vl technical report, 2025.
- [7] Christian Benz, Paul Debus, Huy Khanh Ha, and Volker Rodehorst. Crack segmentation on uas-based imagery using transfer learning. In *2019 International Conference on Image and Vision Computing New Zealand (IVCNZ)*, pages 1–6, 2019.

- [8] Christian Benz and Volker Rodehorst. Image-based detection of structural defects using hierarchical multi-scale attention. In *DAGM German Conference on Pattern Recognition*, pages 337–353. Springer, 2022.
- [9] Eric Bianchi and Matthew Hebdon. Visual structural inspection datasets. *Automation in construction*, 139:104299, 2022.
- [10] Nicolas Carion, Laura Gustafson, Yuan-Ting Hu, Shoubhik Debnath, Ronghang Hu, Didac Suris, Chaitanya Ryali, Kalyan Vasudev Alwala, Haitham Khedr, Andrew Huang, Jie Lei, Tengyu Ma, Baishan Guo, Arpit Kalla, Markus Marks, Joseph Greer, Meng Wang, Peize Sun, Roman Rädle, Triantafyllos Afouras, Effrosyni Mavroudi, Katherine Xu, Tsung-Han Wu, Yu Zhou, Liliane Momeni, Rishi Hazra, Shuangrui Ding, Sagar Vaze, Francois Porcher, Feng Li, Siyuan Li, Aishwarya Kamath, Ho Kei Cheng, Piotr Dollár, Nikhila Ravi, Kate Saenko, Pengchuan Zhang, and Christoph Feichtenhofer. Sam 3: Segment anything with concepts, 2026.
- [11] Nicolas Carion, Francisco Massa, Gabriel Synnaeve, Nicolas Usunier, Alexander Kirillov, and Sergey Zagoruyko. End-to-end object detection with transformers, 2020.
- [12] Christopher Clark, Jieyu Zhang, Zixian Ma, Jae Sung Park, Mohammadreza Salehi, Rohun Tripathi, Sangho Lee, Zhongzheng Ren, Chris Dongjoo Kim, Yinuo Yang, Vincent Shao, Yue Yang, Weikai Huang, Ziqi Gao, Taira Anderson, Jianrui Zhang, Jitesh Jain, George Stoica, Winson Han, Ali Farhadi, and Ranjay Krishna. Molmo2: Open weights and data for vision-language models with video understanding and grounding, 2026.
- [13] Marius Cordts, Mohamed Omran, Sebastian Ramos, Timo Rehfeld, Markus Enzweiler, Rodrigo Benenson, Uwe Franke, Stefan Roth, and Bernt Schiele. The cityscapes dataset for semantic urban scene understanding. In *Proceedings of the IEEE conference on computer vision and pattern recognition*, pages 3213–3223, 2016.
- [14] Matt Deitke, Christopher Clark, Sangho Lee, Rohun Tripathi, Yue Yang, Jae Sung Park, Mohammadreza Salehi, Niklas Muennighoff, Kyle Lo, Luca Soldaini, Jiasen Lu, Taira Anderson, Erin Bransom, Kiana Ehsani, Huong Ngo, YenSung Chen, Ajay Patel, Mark Yatskar, Chris Callison-Burch, Andrew Head, Rose Hendrix, Favyen Bastani, Eli VanderBilt, Nathan Lambert, Yvonne Chou, Arnavi Chheda, Jenna Sparks, Sam Skjonsberg, Michael Schmitz, Aaron Sarnat, Byron Bischoff, Pete Walsh, Chris Newell, Piper Wolters, Tanmay Gupta, Kuo-Hao Zeng, Jon Borchardt, Dirk Groeneveld, Crystal Nam, Sophie Lebrecht, Caitlin Wittlif, Carissa Schoenick, Oscar Michel, Ranjay Krishna, Luca Weihs, Noah A. Smith, Hannaneh Hajishirzi, Ross Girshick, Ali Farhadi, and Aniruddha Kembhavi. Molmo and pixmo: Open weights and open data for state-of-the-art vision-language models, 2024.
- [15] Sattar Dorafshan, Robert J. Thomas, and Marc Maguire. Sdnet2018: An annotated image dataset for non-contact concrete crack detection using deep convolutional neural networks. *Data in Brief*, 21:1664–1668, 2018.
- [16] Charles Farrar and Keith Worden. *Structural Health Monitoring: A Machine Learning Perspective*. John Wiley & Sons, Ltd, 2013.
- [17] Johannes Flotzinger, Philipp J. Rösch, and Thomas Braml. dacl10k: Benchmark for semantic bridge damage segmentation, 2023.
- [18] Robert Geirhos, Patricia Rubisch, Claudio Michaelis, Matthias Bethge, Felix A. Wichmann, and Wieland Brendel. Imagenet-trained cnns are biased towards texture; increasing shape bias improves accuracy and robustness, 2022.
- [19] Philipp Huethwohl. Cambridge bridge inspection dataset, 2017.
- [20] Philipp Hüthwohl, Ruodan Lu, and Ioannis Brilakis. Multi-classifier for reinforced concrete bridge defects. *Automation in Construction*, 105:102824, 2019.
- [21] Tommie Keressies, Niccolò Cavagnero, Alexander Hermans, Narges Norouzi, Giuseppe Averta, Bastian Leibe, Gijs Dubbelman, and Daan de Geus. Your ViT is Secretly an Image Segmentation Model. In *Proceedings of the IEEE/CVF Conference on Computer Vision and Pattern Recognition (CVPR)*, 2025.

- [22] Rahima Khanam and Muhammad Hussain. Yolov11: An overview of the key architectural enhancements. *arXiv preprint arXiv:2410.17725*, 2024.
- [23] Alexander Kirillov, Eric Mintun, Nikhila Ravi, Hanzi Mao, Chloe Rolland, Laura Gustafson, Tete Xiao, Spencer Whitehead, Alexander C. Berg, Wan-Yen Lo, Piotr Dollár, and Ross Girshick. Segment anything, 2023.
- [24] Shreyas Kulkarni, Shreyas Singh, Dhananjay Balakrishnan, Siddharth Sharma, Saipraneeth Devunuri, and Sai Chowdeswara Rao Korlapati. Crackseg9k: A collection and benchmark for crack segmentation datasets and frameworks, 2022.
- [25] Xin Lai, Zhuotao Tian, Yukang Chen, Yanwei Li, Yuhui Yuan, Shu Liu, and Jiaya Jia. Lisa: Reasoning segmentation via large language model, 2024.
- [26] Feng Li, Hao Zhang, Huaizhe Xu, Shilong Liu, Lei Zhang, Lionel M Ni, and Heung-Yeung Shum. Mask dino: Towards a unified transformer-based framework for object detection and segmentation. In *Proceedings of the IEEE/CVF conference on computer vision and pattern recognition*, pages 3041–3050, 2023.
- [27] Feng Li, Renrui Zhang, Hao Zhang, Yuanhan Zhang, Bo Li, Wei Li, Zejun Ma, and Chunyuan Li. Llava-next-interleave: Tackling multi-image, video, and 3d in large multimodal models, 2024.
- [28] Ruiping Li, Linchang Zhao, Hao Wei, Guoqing Hu, Yongchi Xu, Bocheng Ouyang, and Jin Tan. Multi-defect type beam bridge dataset: Gyu-det. *Scientific Data*, 12(1):1101, July 2025.
- [29] Tsung-Yi Lin, Michael Maire, Serge Belongie, James Hays, Pietro Perona, Deva Ramanan, Piotr Dollár, and C. Lawrence Zitnick. Microsoft coco: Common objects in context. In David Fleet, Tomas Pajdla, Bernt Schiele, and Tinne Tuytelaars, editors, *Computer Vision – ECCV 2014*, pages 740–755, Cham, 2014. Springer International Publishing.
- [30] Haotian Liu, Chunyuan Li, Qingyang Wu, and Yong Jae Lee. Visual instruction tuning, 2023.
- [31] Shilong Liu, Zhaoyang Zeng, Tianhe Ren, Feng Li, Hao Zhang, Jie Yang, Qing Jiang, Chunyuan Li, Jianwei Yang, Hang Su, Jun Zhu, and Lei Zhang. Grounding dino: Marrying dino with grounded pre-training for open-set object detection, 2024.
- [32] Arman Malekloo, Ekin Ozer, Mohammad AlHamaydeh, and Mark Girolami. Machine learning and structural health monitoring overview with emerging technology and high-dimensional data source highlights. *Structural Health Monitoring*, 21(4):1906–1955, 2022.
- [33] Brandon McKinzie, Zhe Gan, Jean-Philippe Fauconnier, Sam Dodge, Bowen Zhang, Philipp Dufter, Dhruvi Shah, Xianzhi Du, Futang Peng, Floris Weers, Anton Belyi, Haotian Zhang, Karanjeet Singh, Doug Kang, Ankur Jain, Hongyu Hè, Max Schwarzer, Tom Gunter, Xiang Kong, Aonan Zhang, Jianyu Wang, Chong Wang, Nan Du, Tao Lei, Sam Wiseman, Guoli Yin, Mark Lee, Zirui Wang, Ruoming Pang, Peter Grasch, Alexander Toshev, and Yinfei Yang. Mm1: Methods, analysis & insights from multimodal llm pre-training, 2024.
- [34] Martin Mundt, Sagnik Majumder, Sreenivas Murali, Panagiotis Panetsos, and Visvanathan Ramesh. Meta-learning convolutional neural architectures for multi-target concrete defect classification with the concrete defect bridge image dataset. In *2019 IEEE/CVF Conference on Computer Vision and Pattern Recognition (CVPR)*, pages 11188–11197, 2019.
- [35] Maxime Oquab, Timothée Darcet, Théo Moutakanni, Huy Vo, Marc Szafraniec, Vasil Khalidov, Pierre Fernandez, Daniel Haziza, Francisco Massa, Alaaeldin El-Nouby, Mahmoud Assran, Nicolas Ballas, Wojciech Galuba, Russell Howes, Po-Yao Huang, Shang-Wen Li, Ishan Misra, Michael Rabbat, Vasu Sharma, Gabriel Synnaeve, Hu Xu, Hervé Jegou, Julien Mairal, Patrick Labatut, Armand Joulin, and Piotr Bojanowski. Dinov2: Learning robust visual features without supervision, 2024.
- [36] Çağlar Fırat Özgenel. Concrete crack segmentation dataset. Mendeley Data, V1, 2019.
- [37] Zhiliang Peng, Wenhui Wang, Li Dong, Yaru Hao, Shaohan Huang, Shuming Ma, and Furu Wei. Kosmos-2: Grounding multimodal large language models to the world, 2023.

- [38] Hanoona Rasheed, Muhammad Maaz, Sahal Shaji Mullappilly, Abdelrahman Shaker, Salman Khan, Hisham Cholakkal, Rao M. Anwer, Erix Xing, Ming-Hsuan Yang, and Fahad S. Khan. Glamm: Pixel grounding large multimodal model, 2024.
- [39] Nikhila Ravi, Valentin Gabeur, Yuan-Ting Hu, Ronghang Hu, Chaitanya Ryali, Tengyu Ma, Haitham Khedr, Roman Rädle, Chloe Rolland, Laura Gustafson, Eric Mintun, Junting Pan, Kalyan Vasudev Alwala, Nicolas Carion, Chao-Yuan Wu, Ross Girshick, Piotr Dollár, and Christoph Feichtenhofer. Sam 2: Segment anything in images and videos, 2024.
- [40] Isaac Robinson, Peter Robicheaux, Matvei Popov, Deva Ramanan, and Neehar Peri. Rf-detr: Neural architecture search for real-time detection transformers, 2025.
- [41] Olga Russakovsky, Jia Deng, Hao Su, Jonathan Krause, Sanjeev Satheesh, Sean Ma, Zhiheng Huang, Andrej Karpathy, Aditya Khosla, Michael Bernstein, Alexander C. Berg, and Li Fei-Fei. Imagenet large scale visual recognition challenge, 2015.
- [42] Ranjan Sapkota, Rahul Harsha Cheppally, Ajay Sharda, and Manoj Karkee. Yolo26: key architectural enhancements and performance benchmarking for real-time object detection. *arXiv preprint arXiv:2509.25164*, 2025.
- [43] Christoph Schuhmann, Romain Beaumont, Richard Vencu, Cade Gordon, Ross Wightman, Mehdi Cherti, Theo Coombes, Aarush Katta, Clayton Mullis, Mitchell Wortsman, Patrick Schramowski, Srivatsa Kundurthy, Katherine Crowson, Ludwig Schmidt, Robert Kaczmarczyk, and Jenia Jitsev. Laion-5b: An open large-scale dataset for training next generation image-text models, 2022.
- [44] Oriane Siméoni, Huy V. Vo, Maximilian Seitzer, Federico Baldassarre, Maxime Oquab, Cijo Jose, Vasil Khalidov, Marc Szafraniec, Seungeun Yi, Michaël Ramamonjisoa, Francisco Massa, Daniel Haziza, Luca Wehrstedt, Jianyuan Wang, Timothée Darcet, Théo Moutakanni, Leonel Sentana, Claire Roberts, Andrea Vedaldi, Jamie Tolan, John Brandt, Camille Couprie, Julien Mairal, Hervé Jégou, Patrick Labatut, and Piotr Bojanowski. Dinov3, 2025.
- [45] Zehao Ye, Lucy Lovell, Asaad Faramarzi, and Jelena Ninić. Sam-based instance segmentation models for the automation of structural damage detection. *Advanced Engineering Informatics*, 62:102826, 2024.
- [46] Haoxuan You, Haotian Zhang, Zhe Gan, Xianzhi Du, Bowen Zhang, Zirui Wang, Liangliang Cao, Shih-Fu Chang, and Yinfei Yang. Ferret: Refer and ground anything anywhere at any granularity, 2023.
- [47] Licheng Yu, Patrick Poirson, Shan Yang, Alexander C. Berg, and Tamara L. Berg. Modeling context in referring expressions, 2016.
- [48] Zhaohui Zheng, Yuming Chen, Qibin Hou, Xiang Li, Ping Wang, and Ming-Ming Cheng. Zone evaluation: Revealing spatial bias in object detection, 2024.
- [49] Bolei Zhou, Hang Zhao, Xavier Puig, Sanja Fidler, Adela Barriuso, and Antonio Torralba. Scene parsing through ade20k dataset. In *Proceedings of the IEEE Conference on Computer Vision and Pattern Recognition (CVPR)*, July 2017.

A Technical Appendices and Supplementary Material

A.1 Training Details

All baselines were trained using the off-the-shelf configurations provided in their respective official implementations. The single exception was the YOLOv26-large and YOLOv26-xlarge models, where the default learning rate caused training divergence; consequently, we scaled the learning rate down by an order of magnitude. We consciously refrained from exhaustive hyperparameter optimization. While extensive tuning might yield marginal performance gains, it incurs prohibitive computational costs and unnecessary environmental impact. Furthermore, aggressive tuning falls outside the scope of this work: the primary objective of CiF is to establish global baseline trends and release a large-scale foundational dataset, rather than to overfit specific architectures to the domain.

Due to the scale of the dataset and the number of models evaluated, the experiments required substantial computational resources. All experiments were conducted on the IBM Research internal cluster. The main training phase for the 17 baseline models utilized 17 compute nodes, each equipped with 8 NVIDIA A100 GPUs, for approximately 1 day. Including preliminary experiments, and validation runs, the total project consumed approximately 10,000 NVIDIA A100 GPU hours. All evaluation runs were performed on a single node with 8 NVIDIA A100 GPUs, requiring approximately 2 days.

A.2 Class Co-occurrence

Table 5: Per-class median compactness on the Full variant.

Class	Compactness (median)
Algae	0.69
Crack	0.58
Net-Crack	1.00
Precipitation	0.29
Rust	0.68
Spalling	1.00

Figure 5 reports the normalised frequency with which pairs of defect categories appear in the same image (Full variant).

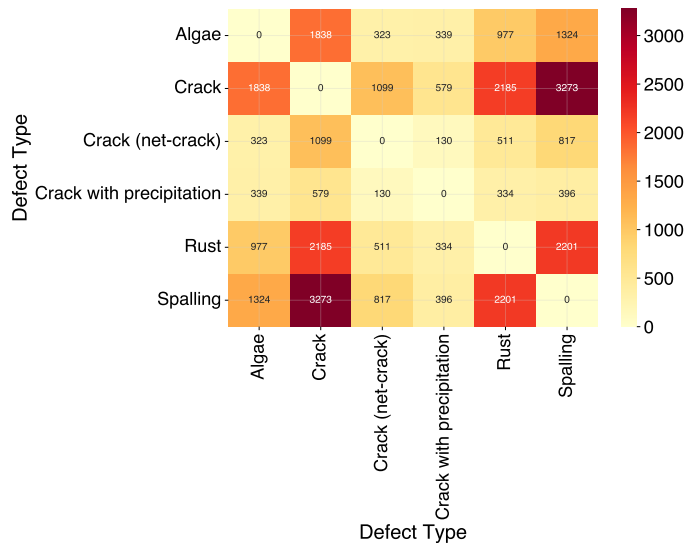


Figure 5: Normalised co-occurrence frequency between defect categories within the same image (Full variant).

A.3 Per-class Shape Compactness

Compactness is the ratio of the instance area to the area of its convex hull, taking values in $[0, 1]$ with values close to 1 indicating convex, blob-like shapes. Table 5 reports per-class median values on the Full variant.

Net-Crack and Spalling are the most compact categories (median 1.00), consistent with their tendency to form simple, convex geometries or polygonal networks. In contrast, Crack with Precipitation has the most irregular boundaries (0.29), driven by diffuse deposition patterns. Crack sits slightly above the midpoint (0.58), reflecting the irregular, branching geometry of individual fractures.